Solar Energy 266 (2023) 112175

Contents lists available at ScienceDirect

Solar Energy

journal homepage: www.elsevier.com/locate/solener

Measurement and analysis of annual solar spectra at different installation angles in central Europe

Guillermo A. Farias-Basulto [a,*], Miguel Á. Sevillano-Bendezú [b], Maximilian Riedel [a], Mark Khenkin [a], Jan A. Töfflinger [b], Rutger Schlatmann [a,c], Reiner Klenk [a], Carolin Ulbrich [a]

[a] PVcomB/ Helmholtz-Zentrum Berlin für Materialien und Energie GmbH, Schwarzschildstr.3, D-12489 Berlin, Germany
[b] Pontificia Universidad Católica del Perú, Department of Sciences, Physics Section, Universitaria Avenue 1801, 15088 Lima, Peru
[c] HTW Berlin - University of Applied Sciences, Wilhelminenhofstr. 75a, D-12459 Berlin, Germany

ARTICLE INFO

Keywords:
Photovoltaics
Solar cell
Solar spectra
Outdoor
Performance
Installation angle

ABSTRACT

The solar spectra in outdoor installations is very seldom equal to that under standard test conditions. This points to the importance of measuring, analyzing and understanding the implications of solar spectra variations with respect to the performance of solar cells. In this work, we present and analyze one year of sun spectra measured at two different angles in central Europe, where the spectrometers were installed at the optimum inclination angle and in vertical orientation, the latter being relevant for building integrated photovoltaics. We report for the first time the differences between the two inclination angles in terms of key performance indicators, such as average photon energy, blue fraction and spectral factor. Moreover, we show the impact of these spectral changes on the maximum current density of ideal single-junction and tandem devices in tilted and vertical orientations. Red-shifted solar spectra were more often found at the vertical installation in comparison to the optimum installation angle, which translated into up to 30% lower current-mismatch losses in idealized tandem devices throughout the year.

1. Introduction

The solar spectrum used for solar cell characterization at standard test conditions (STC) is provided by the international standard IEC 60904-3 [13]. For terrestrial installations, it defines the spectrum assuming an air mass of 1.5 (AM1.5) between the sun and the photovoltaic device, an integrated spectral irradiance of 1000 W/m^2 (AM1.5G), an elevation angle of the sun (zenith angle) of 48.19° and a tilted surface of 37°. The actual solar spectra can be considerably different from the STC spectrum, depending on multiple aspects such as air mass, the position of the sun and the location and geometry of the installation, as well as variations on the atmospheric conditions such as clouds and water vapor. Thus, it is known that the solar spectrum is therefore constantly changing during the day, has seasonal effects and is location specific [6]. These spectral variations have been shown to significantly influence photovoltaic performance [3,4,20,28], which highlights the importance of measuring solar spectral data at specific geographical locations as measured data does not align perfectly with clear-sky models [30], which may be especially significant for systems installed at different angles.

There are numerous parameters and key performance indicators (KPI) that can be used to evaluate and describe solar spectra. Rodrigo et al. [34] have summarized the most widely used indexes related to the quantification of solar spectrum for the performance assessment of photovoltaic systems. Some spectral indexes are completely independent from the actual photovoltaic device, such as the average photon energy (APE) and the blue fraction (BF) [9,25,37], and can be calculated directly from the solar spectrum. However, different PV technologies respond differently to the variation in incident illumination spectrum and the spectral response (SR) of the PV device needs to be considered to estimate the power output of a photovoltaic system in a more precise manner. Therefore, different KPIs, such as the spectral factor (SF) and maximum theoretical electrical current density, are employed [3,5,26,29,34], which depend on physical properties of the photovoltaic device (e.g. band gap).

To our knowledge this work presents for the first time an evaluation and comparison of spectrally resolved irradiance measurements performed in Berlin during a full year (2020) recorded at two angles: close-

* Corresponding author.
E-mail address: guillermo.farias@helmholtz-berlin.de (G.A. Farias-Basulto).

https://doi.org/10.1016/j.solener.2023.112175
Received 4 May 2023; Received in revised form 31 October 2023; Accepted 3 November 2023
Available online 8 November 2023

to-optimum 35° angle and building-integrated photovoltaics (BIPV) relevant angle of 90°. Various KPIs were calculated for both orientations, providing an insight into differences in spectral conditions for vertically installed devices and the theoretical impact on the photogenerated current mismatch in tandem devices.

2. Experimental methods

2.1. Key performance indicators

In this section, various KPIs that are employed in this manuscript are briefly explained. Many definitions were used according to the review paper by Rodrigo et al. [34]. Considering Planck–Einstein relation for the energy of a photon (E_{photon}) and the photon flux (ϕ) for each wavelength (λ) the total global irradiance (G) can be calculated (eq.(1)).

$$G(\lambda) = \phi(\lambda)E_{photon}(\lambda) \tag{1}$$

The widely employed metric named average photon energy (APE) can be calculated. The APE represents the average energy of all photons in a spectrum. APE (in eV) can be calculated using different upper and lower limits, which is described by the integral in Eq. (2), where 'q' is the elementary charge.

$$APE = \frac{\int_{\lambda_1}^{\lambda_2} \mathrm{G}(\lambda)d\lambda}{q\int_{\lambda_1}^{\lambda_2} \phi(\lambda)d\lambda} \tag{2}$$

The blue fraction (BF) can be calculated with Eq. (3). It represents the measure of "blueness" in a solar spectrum by arbitrarily selecting a wavelength 'a' from which it is expected to be half of the total spectrum. This means that a 0.5 value would normally indicate a balanced spectrum. This can change depending on the measured spectrum and on the arbitrary partition wavelength. Typically, a wavelength range between 350 and 1050 nm, and 'a' equal 650 nm, is considered.

$$BF = \frac{\int_{\mathrm{a}}^{\lambda_2} G(\lambda)d\lambda}{\int_{\lambda_1}^{\mathrm{a}} G(\lambda)d\lambda} \tag{3}$$

The spectral factor (SF) is broadly employed to assess the spectral gains or losses due to solar spectrum (G) compared to the global irradiance spectrum at STC (G_{STC} [13]), as represented in Eq. (4), where the integration limits are bound to the wavelength range of the evaluated spectra, the reference spectrum and their spectral response (SR).

$$SF = \frac{\int G(\lambda)SR(\lambda)d\lambda}{\int G_{STC}(\lambda)SR(\lambda)d\lambda} \bullet \frac{\int G_{STC}(\lambda)d\lambda}{\int G(\lambda)d\lambda} \tag{4}$$

The maximum current density (J_{sc}), which a single junction PV device could achieve under a given spectrum is calculated using Eq. (5),

$$J_{sc_i} = \int_{\lambda_1}^{\lambda_2} G_i(\lambda)SR(\lambda)d\lambda, \tag{5}$$

where G_i represents each spectrum and SR is the idealized spectral response. The integrated electric current density can be calculated for specific periods using Eq. (6).

$$J_{sc_{iec}} = \frac{\sum_i J_{sc\,i}}{J_{sc\,STC}} \bullet \frac{G_{STC}}{\sum_i G_i} \tag{6}$$

To facilitate big data handling procedures, the integrals (e.g. (2)) can be modified to a sum by assuming identical intervals within the bottom and top limits. In this work, we use the averaging period of 5 min, as it matches the measurement interval of our spectrometers. Equation (7) represents the general formula for temporal averaging, where 'i' is each interval (measurement or calculation) and 'n' equals the amount of measurements or calculations.

$$\mathrm{KPI}_{Period} = \frac{1}{n}\sum_{i=1}^{n}\mathrm{KPI}_i \tag{7}$$

All the discussed metrics are instantaneous values. They would for example change a lot in the morning and evening hours, when the angle of incidence is very low. However, these changes would not have a large impact on the overall energy yield as the irradiance in morning/evening hours is low. To make our metrics more relevant in terms of energy production, some KPIs were weighted with respect to the global tilted irradiance (GTI) at the moment when they were measured, using Eq. (8),

$$< KPI >_{weighted} = \frac{\sum_1^n (KPI_i * W_i)}{\sum_1^n W_i} \tag{8}$$

where the weight (W_i) is total irradiance over the STC irradiance value of 1000 W/m^2. This weighting method is useful to evaluate the effect of solar spectrum variation on device energy yield, which scales linearly with irradiance.

2.2. Experimental and data processing

Two pairs of spectrometers from *EKO instruments*, installed in our outdoor testing facilities at HZB-PVcomB in Berlin (52°25′52.5″N 13°31′25.7″E), were employed for the measurements presented in this work, each pair consisting of a MS-711 and a MS-712 with a measurement range of 300–1100 nm and 900–1700 nm, respectively (Fig. 1). Both sensors possess an optical (wavelength) resolution (FWHM) smaller than 7 nm, a wavelength accuracy of ± 0.2 nm, an exposure time between 10 and 5000 ms, and a field of view of 180°. Those pairs were installed at both tilt angles, close to optimum (35° degree) angle and the BIPV relevant (90° degree) angle. The measurements were performed in intervals of 5 min.

3. Results

Over 50,000 spectra per spectrometer per angle of installation (i.e. 35° and 90°) were recorded over one full year (2020) in Berlin, which is made available as meta-data [8]. For both angles, the KPIs were calculated in two configurations: Using one spectrometer (MS-711) and limiting the range to 350–1050 nm; and using both spectrometers

Fig. 1. PVcomB-HZB outdoor testing facility showing the two pairs of spectrometers for optimum and vertical angles facing south.

merged with the ranges of 300–1700 nm. Employing both spectrometers is desired as it provides a broader range of information relevant for photovoltaic devices with low band gap (below ~1.18 eV). Thus, the global tilted irradiance (GTI) is related to the latter configuration unless specifically signaled.

3.1. Measurement validation

As validation of our procedure and the spectral data, monthly incident irradiance data at the specific location of our installation were obtained using the photovoltaic geological information system (PVGIS) from the European commission (database: SARAH2, year: 2020) [7], which were compared to the integrated spectra obtained from the merged spectrometer data with no further filtering, but using only physically possible values (i.e. above 0 W/m^2). Fig. 2 shows the total energy per month from PVGIS, as well as from our spectrometers, where some discrepancies in the total absolute value are visible probably due to multiple reasons such as the number of available measurements, a slight difference in azimuth or the complex "city-like" surroundings of the outdoor facilities or possible systematic errors related to different measurement ranges. However, the trends between PVGIS and our spectrometers, especially in the peaks of April and September (in 90°) are unequivocally similar. Moreover, Fig. 2 includes the contribution of direct and diffuse light to the total global irradiance on plane of the array (35° also by PVGIS).

In addition, the measured data were compared to the ideal clear-sky data obtained using the python library, 'clearsky' from the PVlib, where the default Ineichen model methodology was used [14,31]. As expected, the measured irradiance was much lower than those "ideal" values. For the clear sky case (PVlib), the total irradiance received by a vertically installed panel in 2020 was 13 % lower relative to the optimum installation angle, whereas for the on-site spectrometer-measured values it was about 28 % lower, which translates to lower relative efficiencies as shown in literature [20]. Therefore, the simple "clear sky" data were, to the most part, inadequate to forecast energy yield in Berlin, which is also not surprising in view of frequent cloud coverage (and hence high diffuse irradiances) typical for the location. Spectra, which better match different environmental conditions, can be simulated [11,35]. However, in this work, we do not further discuss the meteorological reasons for different spectra, as they have been already studied [10,15,21,25,33,37]. Furthermore, angle dependent penalties, which are aggregated to losses in irradiance, are also not included in this work. Instead, we focus on the implications of solar spectral variations for the two scenarios (35° and 90°).

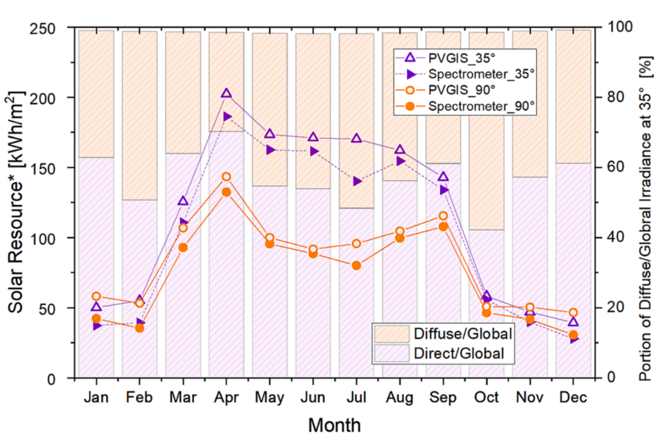

Fig. 2. Monthly solar energy obtained from the integrated measured spectra and from PVGIS using the SARAH2 database. The contribution from direct and diffuse light to the global irradiance is show in orange/purple bars, also calculated using PVGIS. (For interpretation of the references to colour in this figure legend, the reader is referred to the web version of this article.)

3.2. Device independent KPI

To illustrate the differences between simultaneously measured spectra at both angles, Fig. 3 shows merged measurements of the spectrometers (i.e. MS-711 and MS-712), where the solid lines represent the 35° measurements and the dotted lines represent the 90° measurements. To illustrate differences along the year, exemplary single spectra are shown for different months. Discrepancies between the measured spectra and the shape of an AM1.5G spectra can be seen especially during winter months and for low irradiances. The solar spectrum is closer in shape to AM1.5G in summer at an installation angle of 35°. To quantify the differences, we calculated the average photon energy (APE) and the blue fraction (BF) for each of the spectra (refer to the supplementary information; SP: SP1: Table 1).

Fig. 4 shows the data-cloud of all the GTI measured as a function of the APE, which was calculated for 35° tilt angle (in blue) and for 90° tilt angle (in red), showing different peak positions and irradiance ranges. The black solid vertical line represents the APE of the STC spectrum (APE* = 1.6 eV), using the same wavelength limits. For the 35° installation, the APE at the highest irradiation is ~1.62 eV, whereas for the 90° installation, an APE of ~1.55 eV peak was found. The data-clouds suggest that vertically installed solar modules receive more red shifted light compared to the optimal tilt installation. Similar distributions were found for the BF calculations (0.46 and 0.43 peak BF for 35° and 90° angle installation, respectively) indicating that generally in Berlin in 2020, the solar spectra obtained at 35° angles were more blue-rich than at 90° angles.

Spectra with different values of APE and BF but with the same irradiance are also exemplified in Fig. 3. For the 600 W/m^2 case, the black, blue and red lines had APEs of 1.54, 1.56 and 1.66 eV, respectively; whereas for the 100 W/m^2 case, the green, purple and orange lines result in values of 1.4, 1.62 and 1.85 eV, respectively. It is worth noticing that the difference in APE can be much larger for the 100 W/m^2 case as depicted in Fig. 4. Therefore, it is evident from Fig. 3 that the lower the irradiance, the more likely the APE and BF will vary over a larger range, which can happen due to significant deviations from AM1.5 as seen in Fig. 4.

The statistical mean values of the average photon energies and blue fractions over the year for both angles, are visualized in Fig. 5. The results can be compared to the provided references (purple horizontal lines), which were extracted using the same procedures with the AM1.5G spectrum and which are shown for two configurations: single spectrometer (1S) and merged spectrometers (2S). For comparison, values of APE and BF calculated using the widely employed integration range of 350–1050 nm are presented in the supplementary information (SP2: Table 2). For the single spectrometer configuration, the APE and BF values at 90°, relative to the 35° installation angle, present a relative decrease of 1.6 % and 4.3 %, respectively. When employing both spectrometers, the discrepancy caused by data dispersion towards low irradiances (see Fig. 4) can be reduced by calculating the APE and BF weighted proportionally to the irradiance, which can be seen by comparing the standard deviation reduction (represented by the whiskers) in Fig. 5. Therefore, we concluded that the weighted KPI is preferred for the evaluation using both spectrometers. Statistical mean ⟨APE⟩ values over the year decrease from 1.64 to 1.60 eV going from the optimal (35°) to vertical (90°) installation angle (⟨BF⟩ changes from 0.449 to 0.419). This indicates that, in comparison to the reference AM1.5G spectrum used indoors by most researchers, which for the BF represents the threshold between blue and red shifted spectra, the outdoor solar spectra are slightly blue-shifted in the optimal orientation, but red-shifted in the vertical orientation.

As expected from literature [25,37], the BF and the APE also change seasonally, having similar trends. This can be seen in Fig. 6, where the GTI is also included. Fig. 6 depicts the < APE> (in black), <BF> (in red) and global irradiance (GTI) (in blue) values for the 35° (solid dots and lines) and 90° (void dots and dashed lines) installation angles, where the

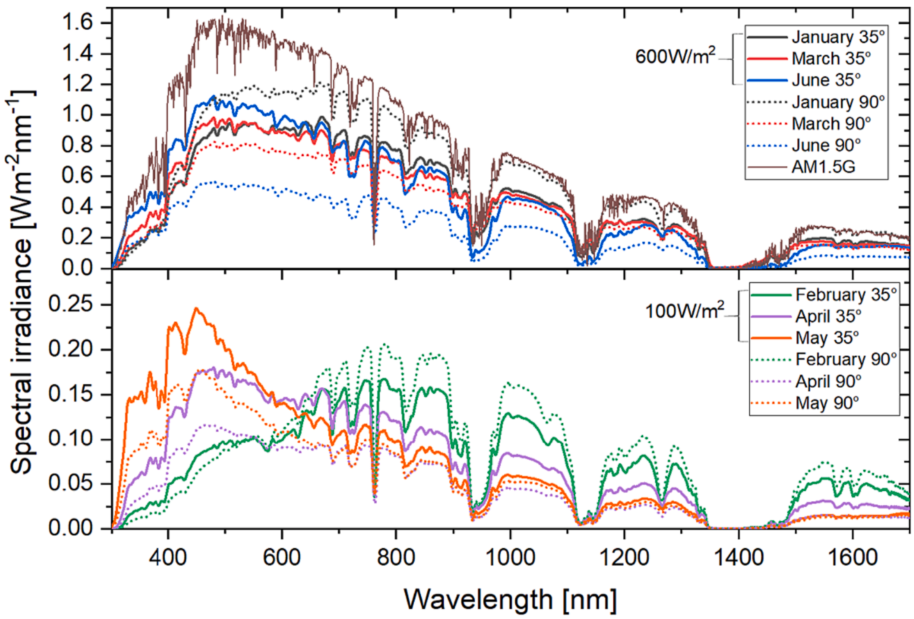

Fig. 3. Solar spectra example measurements at two different installation angles: 35° (solid lines) and 90° (dotted lines).

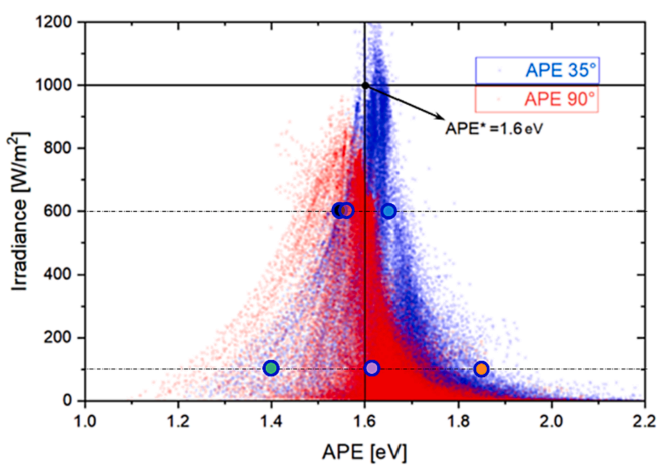

Fig. 4. Data-cloud of calculated average photon energies (APE) from measured spectra incident in 35° and 90° installation tilt angles in Berlin over a year, showing six data points highlighted for exemplification of the spectra shown in Fig. 3.

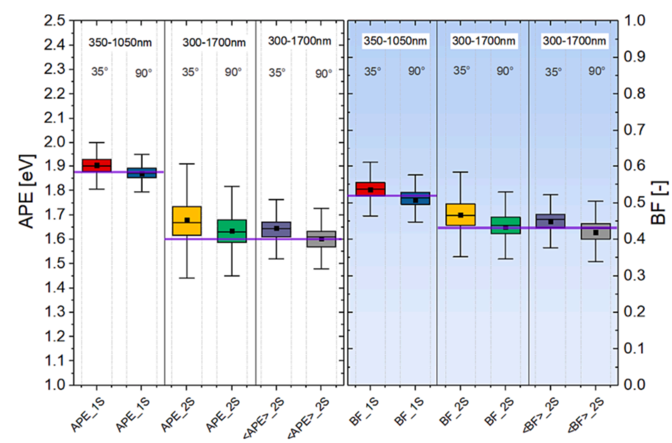

Fig. 5. Box plot of APE and BF average values for the year 2020 using only one spectrometer (1S) or both spectrometers (2S) for two installation angles angles (35° and 90°). ⟨APE⟩ and ⟨BF⟩ represent irradiance weighted values. The purple lines correspond to the STC spectrum. (For interpretation of the references to colour in this figure legend, the reader is referred to the web version of this article.)

reference values (using the STC spectrum) are indicated by straight horizontal lines. In Berlin, summer solar spectra are significantly blue shifted compared to winter. Higher average monthly values of ⟨APE⟩ and ⟨BF⟩ from 35° with respect to 90° installation angle are evident in every month, even when the irradiances are similar.

In addition, some general trends for both angles can be seen. Using a principal component analysis, the aforementioned correlation between ⟨BF⟩ and ⟨APE⟩ can be obtained quantitatively (96.78 % correlation). Furthermore, there is a seemingly inverse correlation (−45 %) between GTI and ⟨APE⟩. This can be identified in Fig. 6 by following the months of April to September, where the ⟨APE⟩ and ⟨BF⟩ increase as the irradiance decreases. On one hand, the global tilted irradiance, the ⟨APE⟩ and the ⟨BF⟩ should all increase as the elevation angle of the sun increases. On the other hand, the discrepancies between measured and ideal irradiances suggest that Berlin had a generally cloudy summer in 2020. It has been found in literature that cloudy weather can cause high APE [15], which can be related to a large diffuse irradiance [21] (as seen in Fig. 2), and which could explain the larger ⟨APE⟩ values in February and October.

3.3. Photovoltaic device dependent KPI

For this section, all the calculations involving different band gaps were done assuming ideal photovoltaic devices (abrupt transition from 100 % to 0 quantum efficiency at the band gap). Only band gaps relatively close to commonly employed photovoltaic absorber materials (i.e. between 1.0 and 1.7 eV) in the PV industry were considered.

3.3.1. Spectral factor

Fig. 7 shows the irradiance-weighted spectral factor (⟨SF⟩) average values in 2020 for both 35° and 90° inclination angles for different band gaps. To prevent large angular influences and to reduce noisy measurements, SF data below an irradiance angle of incidence of 60° and below 25 W/m^2 were filtered out. The ⟨SF⟩ yearly average values show, generally, increasing gains as the band gap increases for the 35°

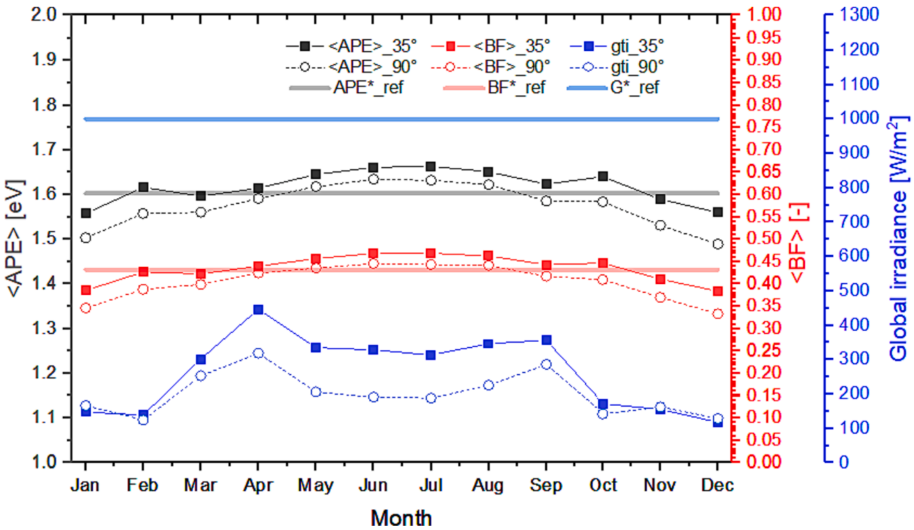

Fig. 6. Monthly weighted statistical means of measured global tilted irradiance, ⟨APE⟩ and ⟨BF⟩ for the year 2020 for the two compared angles of close to optimum 35° and BIPV relevant 90°.

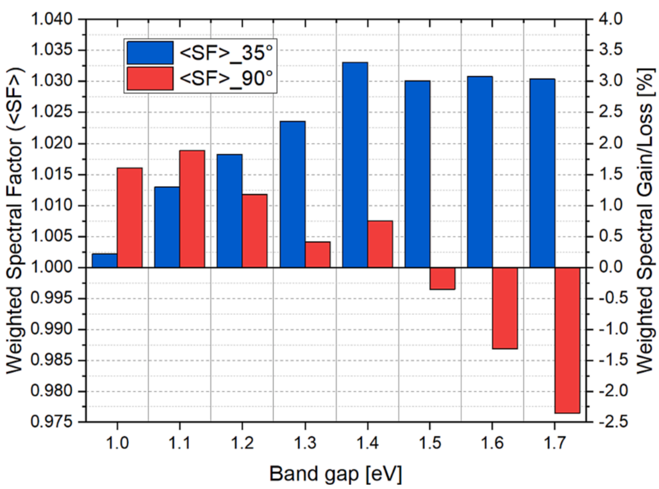

Fig. 7. Year average ⟨SF⟩ of ideal single junction PV devices for 35° and 90° installation angles for different band gaps.

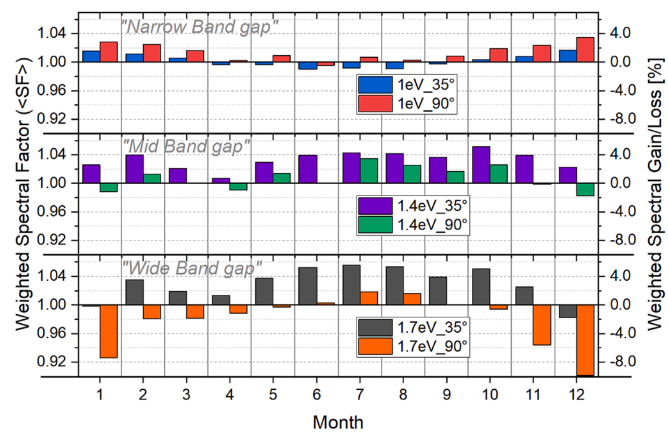

Fig. 8. Monthly average weighted spectral factor of ideal single-junction PV devices for 35° and 90° installation angles for different band gaps.

installation (blue bars). However, the opposite trend is visible for the 90° installation (red bars), starting from a positive spectral gain of about 1.5 % for 1.0 eV to a loss of about 2.3 % for 1.7 eV, which can be explained by the red dominated spectra in the 90° angle installation.

The total relative GTI losses found at a 90° relative to the 35° installation angle in 2020 were about 28 %. According to our calculations, this could be slightly mitigated (~1.5 %) for low band gap materials such as silicon or CIGS (i.e.1.0–1.1 eV). However, at a band gap of about 1.2 eV and above, the 28 % GTI difference is augmented by the ⟨SF⟩ up to more than 5 % (relative) due to the red-shifted solar spectrum. In addition, the average ⟨SF⟩ values for both installations change monthly as expected, which is represented in Fig. 8. To facilitate visualization, only the band gaps of 1.0, 1.4 and 1.7 eV were included. In general, for wide band gap materials (e.g. 1.7 eV), the average ⟨SF⟩ increases towards summer and decreases towards winter due to a larger distribution of redder spectra in winter, which can be seen already in Fig. 6.

As narrow band gap solar cells (e.g. 1.0 eV) are sensitive to most of the spectral range, low variance of SF is expected [10]. Nevertheless, the red-shifted spectra, due to the 90° angle and winter season, show to be beneficial as the weighted spectral gain seems to slightly increase towards winter, possibly related to much lower irradiances during these period than the typically low irradiances found for the climate zone of Berlin [1]. The mid-band gap case (e.g. 1.4 eV), being the optimum wavelength for one-junction photovoltaic STC efficiency, appears to have no spectral losses for the 35° installation angle and follows similar trends as the wide band gap material scenario.

3.3.2. *Maximum current density*

In this section, the maximum short circuit current density (Jsc in mA/cm^2), was calculated (per spectrum), where the assumption of an ideal PV, as in the previous section, is considered.

- *Single Junction devices*

As the variation in irradiance (and its proportional change in photocurrent and power) influences the performance of solar cells [3,5,9,20], it is interesting to address the intra-day variation of the maximum theoretical current for the two evaluated angles together with the possible gains or losses due to spectral variation. Fig. 9 shows the average intra-day variation of the J_{sc}, where the “average day” for each month represents the average J_{sc} calculated for all recorded spectra during a specific time of the day for all 5 min time intervals (e.g. in January, 31 measurements at the 8:00–8:05am interval) for the two

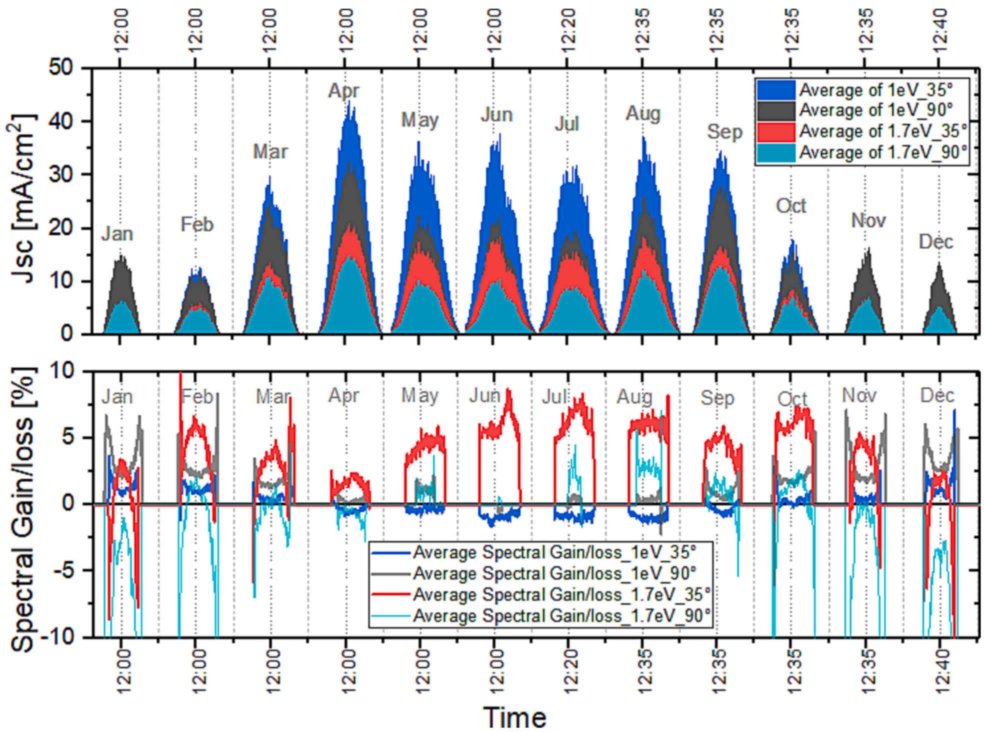

Fig. 9. Intraday average per month (Year 2020) of Jsc of ideal single-junction PV devices for 35° and 90° installation angles calculated for two band gaps (1.0 and 1.7 eV).

evaluated angles and two band gaps (1.0 eV and 1.7 eV). As expected, lower band gap and optimal installation angle resulted in overall higher J_{sc}.

Furthermore, Fig. 9 also includes the intraday energy gains or losses due to spectral variations, showing the opposite trends depending on the band gap. In agreement with Fig. 7, spectral effects had higher magnitude for wide band gap devices. Spectral gains for low band gap devices installed vertically were very pronounced in winter months and almost negligible from April to August. This was due to the relatively blue rich spectrum in summer in Berlin compared to winter. The ideal solar devices with a wide band gap of 1.7 eV installed at optimum angle (in red), had spectral gains, which were more strongly expressed in summer. Installing such device vertically (shown in cyan), and therefore exposing it to redshifted light, resulted in much lower gains in summer and even losses in winter.

From the total current generated for each scenario, the spectral gains or losses correlate to the ones presented in Fig. 7, for instance, on average the 1.0 eV device provides slightly more spectral gain at a 90° angle (1.8 % more Jsc due partially to the larger gains in winter) in contrast to the 35°case (0.02 %), whereas for the 1.7 eV case, a 35° installation angle is more beneficial (4.21 % more Jsc) in contrast to the vertical installation (2.52 % less Jsc).

The intraday variations of the photo-generated current might be, depending on the band gap, trivial for single junction devices. However, changes in the IV parameters become significant for the performance of tandem devices [17]. To investigate the role of the afore-mentioned intra-daily current variation, we have broadened our calculations for a two-junction tandem device.

- *Tandem devices*

For the two-junction tandem-device evaluation, the Jsc was calculated using a similar approach as for the Z-parameter [26,29,34]. However, our results are calculated for each spectrum using the photocurrent mismatch ratio (J_{sc_MM}), which represents the mismatch between top and bottom cells relative to the theoretical total available photocurrent (Eq. (9)),. Therefore, each incident spectrum measured, for each installation angle, was separated into top cell and bottom cell with the aforementioned assumptions.

$$J_{sc_{MM}} = \left(\frac{J_{sc\,top} - J_{sc_{bottom}}}{J_{sc\,top} + J_{sc_{bottom}}}\right) \bullet 100\,\% \tag{9}$$

Fig. 10 presents the J_{sc_MM} for three different devices for the two installation scenarios, where zero denotes the threshold between top limited and bottom limited, assuming a current-matched 2-terminal ideal tandem-device. Therefore, regardless of whether the device is subject to top- or bottom-cell limited behavior, any deviation from a perfectly current-matched device (i.e. $J_{sc\_MM} = 0$) results in performance losses. The first device "T1" represents a device similar to a CIGS-Perovskite tandem (i.e. 1.0–1.65 eV) [19]. The second device "T2"

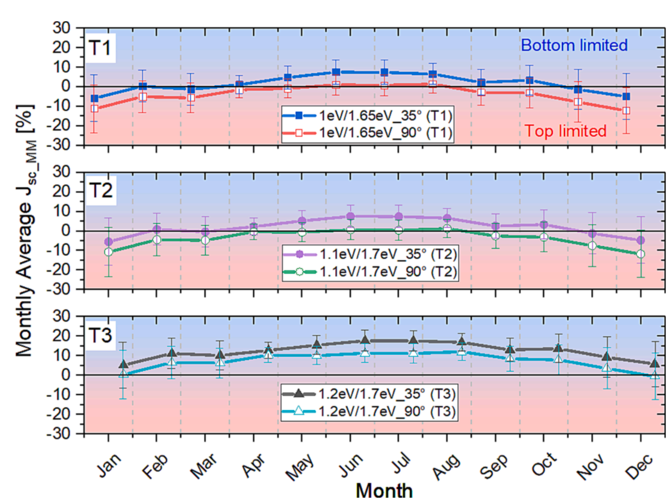

Fig. 10. Monthly average (year 2020) of J_{sc_MM} of various ideal PV tandem devices installed at 35° and 90° angles.

represents a device similar to a tandem using CIGS [18,16] or c-Si as bottom (i.e. ~1.1 eV) and Perovskite (i.e. 1.7 eV) as top device [23,22,27,36]. The third device "T3" embodies a device relating to a Perovskite-Perovskite tandem [2,12,24,32].

As previously discussed, vertically installed devices receive, on average, larger amounts of redshifted solar spectra than the ones installed at an optimum angle. This in turn, as seen in Fig. 10, leads to higher current generated in the bottom cell and lower current generated in the top cell. As a result, tandems installed vertically are top cell limited for the most part of the year (red areas in Fig. 10), whereas tandems installed at optimum angle are mostly top cell limited (blue areas in Fig. 10) (for 1.2 eV/1.7 eV band gap combination it is even true for the entire year in Berlin). Furthermore, the J_{sc_MM} generally changes towards more positive values as the elevation of the sun increases, which is expected due to the bluer spectra (e.g. Fig. 6), whereas, as the elevation of the sun decreases, the J_{sc_MM} generally changes toward more negative values.

In other words, two-junction tandem devices tend to be top-limited towards the summer solstice and bottom-limited towards the winter solstice. Device 'T3' (i.e. 1.2/1.7 eV) shows a much more bottom-cell-limited behavior due to the relatively wide band gap of the bottom cell, in comparison to T1 and T2. This reflects the less ideal combination of band gaps given in this device in general.

$$Mean\ Energy\ Loss = \frac{1}{n}\sum_{i}^{n}\left|J_{scMM_i}\right| \tag{10}$$

From the data in Fig. 10, we have calculated the theoretical mean annual losses due to spectral mismatch (Eq. (10)). In the presented two-terminal tandem scenarios, the average energy loss related to current mismatch are relatively smaller in the 90° installation angle by 20, 26 and 30 % for T1, T2 and T3, respectively. For instance, the mean energy losses due current mismatch for the T2 device throughout the year were 6.4 % and 4.7 %, for 35° and 90°, respectively. This opens a good perspective for this type of devices in BIPV applications in particular.

Hence, the different angles have a clear impact in performance, which can be especially significant for tandem devices. This impact can be exemplified further with the intra-day average of J_{sc_MM}. Fig. 11 shows the intraday variation for the 'T2' device (i.e. 1.1/1.7 eV) for 35° and 90° installations, demonstrating possible energy losses due to current mismatch as the elevation of the sun progresses. It is worth noticing that the variation in performance is larger for the 90° case, as shown in literature using similar devices [20]. However, as photo-generated current during these periods is normally lower, due to lower irradiances in winter, the overall mismatch losses were, as previously stated, smaller.

While it was previously stated that the 90° signifies multiple yield penalties (irradiance, angle dependent and spectral losses), it could mediate slightly some of the current mismatch losses in a tandem, as implied by Fig. 11. By using a 90° tilt, the mismatch losses due to the bluer spectra could be reduced, which would be beneficial for the performance of tandem devices.

4. Conclusions

In this work, we analyzed variations in solar spectra from January to December of 2020 and their implications for PV devices installed at optimum angle (as in PV power plants) and vertically (as in building-integrated PV applications) in Berlin. For this, sets of spectrometers were installed in both orientations, providing over 50,000 measurements per spectrometer per angle, which were validated by comparison of the integrated irradiances to measurements of incident irradiance performed, in the same timeframe and independently, by the European Commission.

As anticipated, we observed that changing the angle of installation not only reduces the total irradiance received (~28 % less irradiance in vertical installation in 2020), which is the major downside for PV

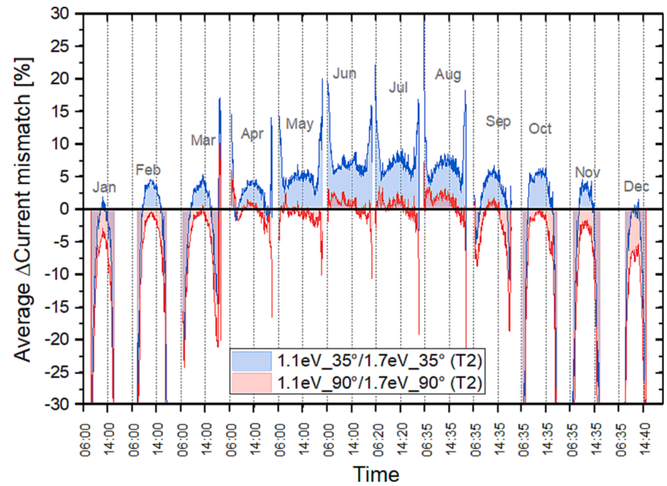

Fig. 11. Intraday average (year 2020) per month of J_{sc} of an ideal PV tandem device with a bottom cell of 1.1 eV and a top cell of 1.7 eV installed at 35° and 90° angles.

performance, but also significantly affects its spectral distribution. In general, devices in vertical orientation receive a red-shifted light (lower APE and BF) compared to those installed under optimum angle, mostly due to higher fraction of diffuse light. For single-junction devices with narrow band gap (e.g. 1.0 eV) this results in slightly larger spectral gains for the 90° in comparison to the 35° angle installation (~1.5 % absolute), whereas for wide band gaps (e.g. 1.7 eV), much larger spectral gains were obtained for the 35° installation (5.5 % absolute). However, in terms of Jsc alone and for single-junction devices, due to the aforementioned irradiance losses, the 35° angle installation in combination with a lower bandgap is preferred.

The current-mismatch in ideal two-terminal tandem devices due to spectral variation in both orientations was evaluated. Changes in the solar spectrum over the year lead to the aforementioned mismatch and, therefore, to considerable current losses (e.g. for the T2 scenarios, 6.4 % and 4.7 % for 35° and 90°, angles respectively), which are caused, on average, from top-cell limitation in winter and bottom cell limitation in summer. These changes are relatively less pronounced for devices installed at 90° angles (a relative 20 %, 26 % and 30 % for scenarios T1, T2 and T3), which is beneficial for BIPV, given that, overall, vertically installed devices experience less (significant) incident irradiance variation over the year, which lowers intra-day and seasonal changes in PV power output overall.

Declaration of Competing Interest

The authors declare that they have no known competing financial interests or personal relationships that could have appeared to influence the work reported in this paper.

Acknowledgments

Carolin Ulbrich acknowledges support by the Helmholtz Association under the program "Energy System Design" under grant number ZT-0002.

M. Riedel and M. Khenkin acknowledge the support of European partnering protect TAPAS (PIE-0015).

M. A. Sevillano-Bendezú acknowledges the doctoral scholarship of CONCYTEC through PROCIENCIA, contract N°236-2015-FONDECYT.

Appendix A. Supplementary data

Supplementary data to this article can be found online at https://doi.org/10.1016/j.solener.2023.112175.

References

[1] J. Ascencio-Vásquez, K. Brecl, M. Topič, Methodology of Köppen-Geiger-Photovoltaic climate classification and implications to worldwide mapping of PV system performance, Sol. Energy 191 (2019) 672–685, https://doi.org/10.1016/j.solener.2019.08.072.

[2] A.S.R. Bati, Y.L. Zhong, P.L. Burn, M.K. Nazeeruddin, P.E. Shaw, M. Batmunkh, Next-generation applications for integrated perovskite solar cells, Commun Mater 4 (2023) 2, https://doi.org/10.1038/s43246-022-00325-4.

[3] J. Bonilla Castro, M. Schweiger, D. Moser, T. Tanahashi, B.H. King, G. Friesen, L. Haitao, R. French, L.S. Bruckman, B. Miiller, C. Reise, G. Eder, W. van Sark, Y. Sangpongsanon, F. Valencia, J.S. Stein, Integration of Photovoltaic Solar Energy, E. and R., Climatic Rating of Photovoltaic Modules: Different Technologies for Various Operating Conditions. IEA-PVPS (2020).

[4] D. Dirnberger, G. Blackburn, B. Müller, C. Reise, On the impact of solar spectral irradiance on the yield of different PV technologies, Sol. Energy Mater. Sol. Cells 132 (2015) 431–442, https://doi.org/10.1016/j.solmat.2014.09.034.

[5] D. Dirnberger, B. Müller, C. Reise, PV module energy rating: opportunities and limitations: PV module energy rating: opportunities and limitations, Prog. Photovolt. Res. Appl. 23 (2015) 1754–1770, https://doi.org/10.1002/pip.2618.

[6] Y.A. Eltbaakh, M.H. Ruslan, M.A. Alghoul, M.Y. Othman, K. Sopian, M.I. Fadhel, Measurement of total and spectral solar irradiance: Overview of existing research, Renew. Sustain. Energy Rev. 15 (2011) 1403–1426, https://doi.org/10.1016/j.rser.2010.10.018.

[7] European Commission. JRC Photovoltaic Geographical Information System (PVGIS) - European Commission [WWW Document] (2019). URL https://re.jrc.ec.europa.eu/pvg_tools/en/tools.html#MR (accessed 4.23.20).

[8] G.A. Farias-Basulto, Solar spectra datasets at optimum and vertical installation angles in central Europe (Berlin) during 2020, 2021 and 2022 (2023). 10.1016/j.dib.2023.109273.

[9] G. Friesen, W. Herrmann, G. Belluardo, B. Herteleer, Photovoltaic Module Energy Yield Measurements: Existing Approaches and Best Practice (2018).

[10] R. Gottschalg, D.G. Infield, M.J. Kearney, Experimental study of variations of the solar spectrum of relevance to thin film solar cells, Sol. Energy Mater. Sol. Cells 79 (2003) 527–537, https://doi.org/10.1016/S0927-0248(03)00106-5.

[11] C.A. Gueymard, The SMARTS spectral irradiance model after 25 years: New developments and validation of reference spectra, Sol. Energy 187 (2019) 233–253, https://doi.org/10.1016/j.solener.2019.05.048.

[12] F. Hao, C.C. Stoumpos, R.P.H. Chang, M.G. Kanatzidis, Anomalous band gap behavior in mixed Sn and Pb perovskites enables broadening of absorption spectrum in solar cells, J. Am. Chem. Soc. 136 (2014) 8094–8099, https://doi.org/10.1021/ja5033259.

[13] IEC. IEC 60904-3:2019. Photovoltaic devices - Part 3: Measurement principles for terrestrial photovoltaic (PV) solar devices with reference spectral irradiance data (2019).

[14] P. Ineichen, R. Perez, A new airmass independent formulation for the Linke turbidity coefficient (2002). 10.1016/S0038-092X(02)00045-2.

[15] T. Ishii, K. Otani, T. Takashima, Y. Xue, Solar spectral influence on the performance of photovoltaic (PV) modules under fine weather and cloudy weather conditions: Solar spectral influence on the performance of photovoltaic (PV) modules, Prog. Photovolt: Res. Appl. (2011), https://doi.org/10.1002/pip.1210.

[16] M. Jošt, T. Bertram, D. Koushik, J.A. Marquez, M.A. Verheijen, M.D. Heinemann, E. Köhnen, A. Al-Ashouri, B. Rech, T. Unold, M. Creatore, I. Lauermann, C. A. Kaufmann, R. Schlatmann, S. Albrecht, Highly efficient monolithic perovskite/CIGSe tandem solar cells on rough bottom cell surfaces, in: 2019 IEEE 46th Photovoltaic Specialists Conference (PVSC). Presented at the 2019 IEEE 46th Photovoltaic Specialists Conference (PVSC), 2019, pp. 0738–0742, https://doi.org/10.1109/PVSC40753.2019.8980493.

[17] M. Jošt, L. Kegelmann, L. Korte, S. Albrecht, Monolithic perovskite tandem solar cells: A review of the present status and advanced characterization methods toward 30% efficiency, Adv. Energy Mater. 10 (2020), 1904102, https://doi.org/10.1002/aenm.201904102.

[18] M. Jošt, E. Köhnen, A. Al-Ashouri, T. Bertram, Š. Tomšič, A. Magomedov, E. Kasparavicius, T. Kodalle, B. Lipovšek, V. Getautis, R. Schlatmann, C. A. Kaufmann, S. Albrecht, M. Topič, Perovskite/CIGS tandem solar cells: from certified 24.2% toward 30% and beyond, ACS Energy Lett. 7 (2022) 1298–1307, https://doi.org/10.1021/acsenergylett.2c00274.

[19] I. Kafedjiska, G.A. Farias-Basulto, P. Reyes-Figueroa, T. Bertram, A. Al-Ashouri, C. A. Kaufmann, R. Wenisch, S. Albrecht, R. Schlatmann, I. Lauermann, Integration of rough RTP absorbers into CIGS-perovskite monolithic tandems by NiOx(:Cu)+SAM Hole-transporting Bi-layers, Sol. Energy Mater. Sol. Cells 254 (2023), 112248, https://doi.org/10.1016/j.solmat.2023.112248.

[20] G.S. Kinsey, M. Boyd, M. Braga, N.C. Riedel-Lyngskær, R.R. Cordero, B.C. Duck, C. J. Fell, S. Feron, G.E. Georghiou, N. Ketjoy, A. Louwen, T. Minemoto, G. Neves, G. N. Garrido, B.R. Paudyal, C.D.R. Gallegos, R. Rüther, W. van Sark, M.A. Sevillano-Bendezú, M. Theristis, J.A. Töfflinger, M.A. Yamasoe, M. Alonso-Abella, S. Chunhui, N. Habryl, J.J. John, G. López, L. Maweza, A. Mittal, C. Molto, M. Norton, E.B. Pereira, Y. Poissant, L. Pratt, S. Qu, T. Reindl, M. Rennhofer, H. Seigneur, J.A. Tejero, C. Ulbrich, W.A. Vilel, X. Xia, Impact of measured spectrum variation on solar photovoltaic efficiencies worldwide (2022). 10.31224/osf.io/t5hu3.

[21] B. Kirn, M. Topič, Diffuse and direct light solar spectra modeling in PV module performance rating (2017). 10.1016/J.SOLENER.2017.04.047.

[22] E. Köhnen, M. Jošt, A.B. Morales-Vilches, P. Tockhorn, A. Al-Ashouri, B. Macco, L. Kegelmann, L. Korte, B. Rech, R. Schlatmann, B. Stannowski, S. Albrecht, Highly efficient monolithic perovskite silicon tandem solar cells: analyzing the influence of current mismatch on device performance, Sustain. Energy Fuels 3 (2019) 1995–2005, https://doi.org/10.1039/C9SE00120D.

[23] E. Köhnen, P. Wagner, F. Lang, A. Cruz, B. Li, M. Roß, M. Jošt, A.B. Morales-Vilches, M. Topič, M. Stolterfoht, D. Neher, L. Korte, B. Rech, R. Schlatmann, B. Stannowski, S. Albrecht, 27.9% efficient monolithic perovskite/silicon tandem solar cells on industry compatible bottom cells, Solar RRL 5 (2021) 2100244, https://doi.org/10.1002/solr.202100244.

[24] W. Liao, D. Zhao, Y. Yu, N. Shrestha, K. Ghimire, C.R. Grice, C. Wang, Y. Xiao, A. J. Cimaroli, R.J. Ellingson, N.J. Podraza, K. Zhu, R.-G. Xiong, Y. Yan, Fabrication of efficient low-bandgap perovskite solar cells by combining formamidinium tin iodide with methylammonium lead iodide, J. Am. Chem. Soc. 138 (2016) 12360–12363, https://doi.org/10.1021/jacs.6b08337.

[25] A. Louwen, A.C. de Waal, W.G.J.H.M. van Sark, Evaluation of different indicators for representing solar spectral variation, in: IEEE 43rd Photovoltaic Specialists Conference (PVSC). Presented at the 2016 IEEE 43rd Photovoltaic Specialists Conference (PVSC), IEEE, Portland, OR, USA, 2016, pp. 0133–0137, https://doi.org/10.1109/PVSC.2016.7749563.

[26] M. Meusel, R. Adelhelm, F. Dimroth, A.W. Bett, W. Warta, Spectral mismatch correction and spectrometric characterization of monolithic III-V multi-junction solar cells, Prog. Photovolt: Res. Appl. 10 (2002) 243–255, https://doi.org/10.1002/pip.407.

[27] B. Minnaert, P. Veelaert, Guidelines for the bandgap combinations and absorption windows for organic tandem and triple-junction solar cells, Materials 5 (2012) 1933–1953, https://doi.org/10.3390/ma5101933.

[28] G. Neves, W. Vilela, E. Pereira, M. Yamasoe, G. Nofuentes, Spectral impact on PV in low-latitude sites: The case of southeastern Brazil, Renew. Energy 164 (2021) 1306–1319, https://doi.org/10.1016/j.renene.2020.10.128.

[29] G. Peharz, G. Siefer, A.W. Bett, A simple method for quantifying spectral impacts on multi-junction solar cells, Sol. Energy 83 (2009) 1588–1598, https://doi.org/10.1016/j.solener.2009.05.009.

[30] S. Pelland, C.A. Gueymard, Validation of photovoltaic spectral effects derived from satellite-based solar irradiance products, IEEE J. Photovoltaics 12 (2022) 1361–1368, https://doi.org/10.1109/JPHOTOV.2022.3216501.

[31] R. Perez, P. Ineichen, K. Moore, M. Kmiecik, C. Chain, R. George, F. Vignola, A new operational model for satellite-derived irradiances: description and validation, Sol. Energy 73 (2002) 307–317, https://doi.org/10.1016/S0038-092X(02)00122-6.

[32] R. Prasanna, A. Gold-Parker, T. Leijtens, B. Conings, A. Babayigit, H.-G. Boyen, M. F. Toney, M.D. McGehee, Band gap tuning via lattice contraction and octahedral tilting in perovskite materials for photovoltaics, J. Am. Chem. Soc. 139 (2017) 11117–11124, https://doi.org/10.1021/jacs.7b04981.

[33] N. Reiners, U. Blieske, S. Siebentritt, Investigation on the angle and spectral dependence of the internal and the external quantum efficiency of crystalline silicon solar cells and modules, IEEE J. Photovoltaics 8 (2018) 1738–1747, https://doi.org/10.1109/JPHOTOV.2018.2860956.

[34] P.M. Rodrigo, E.F. Fernández, F.M. Almonacid, P.J. Pérez-Higueras, Quantification of the spectral coupling of atmosphere and photovoltaic system performance: Indexes, methods and impact on energy harvesting, Sol. Energy Mater. Sol. Cells 163 (2017) 73–90, https://doi.org/10.1016/j.solmat.2017.01.018.

[35] Solar Consulting Services [WWW Document], n.d. URL https://www.solarconsultingservices.com (accessed 10.27.23).

[36] P. Tockhorn, J. Sutter, A. Cruz, P. Wagner, K. Jäger, D. Yoo, F. Lang, M. Grischek, B. Li, A. Al-Ashouri, E. Köhnen, M. Stolterfoht, D. Neher, R. Schlatmann, B. Rech, B. Stannowski, S. Albrecht, C. Becker, Nano-optical designs enhance monolithic perovskite/silicon tandem solar cells toward 29.8% efficiency (preprint). In Review (2022). 10.21203/rs.3.rs-1439562/v1.

[37] B. Zinßer, M.B. Schubert, J.H. Werner, Spectral dependent annual yield of different photovoltaic technologies, in: Presented at the 26th European Photovoltaic Solar Energy Conference and Exhibition, Shaker Verlag GmbH, DE, 2011, pp. 3615–3618, https://doi.org/10.4229/26thEUPVSEC2011-4AV.2.42.